Draft version December 1, 2023
Typeset using LaTeX **twocolumn** style in AASTeX631

Hertzsprung-Russell Diagram of M52 revealed by DoA Dome Telescope

Jin Bingcheng[1]

[1]*Department of Astronomy, School of Physics, Peking University, Beijing 100871, China*

ABSTRACT

I present the data reduction process and final results for DoA Dome Telescope observations for M52 during few nights in September. These data consist of Optical imaging in three broadband filters (B, V, sdss-r) over all pointings. I reduced the imaging data with a self-bulit Calibration Pipeline, with custom modifications and reduction steps designed to address additional features and challenges with the data. Here I provide a detailed description of each step in my reduction and a discussion of final measurement results. The final results are Hertzsprung-Russell Diagram for M52. I compare my data with previous measurement and the result shows consistentency.

Keywords: Star Clusters, Imaging, Data Reduction, WCS Calibration, Flux Calibration, Hertzsprung-Russell Diagram

1. INTRODUCTION

In September 2023, the class OBS 2023 used DoA Dome telescope to observe several star clusters. The observing schedule includes Globular Clusters M92, M15, M13, and Open Clusters M52, M11. The scientific goal of this observation is to measure the color and brightness distribution of stellar members in these clusters, i.e., Hertzsprung-Russell Diagram. To achieve this goal, My report is structured as follows. In Section 2, I will describe the observation and data acquisition. In Section 3, I present my own data reduction process, which is a custom pipeline for image reduction, and slightly different from the variable reduction pipeline. In Section 4, I will point out the known issues in the data reduction. In Section 5, the final results is presented. In Section 6, I will finally discuss the results and comparison with previous measurement.

2. DOA DOME TELESCOPE OBSERVATIONS

The DoA Dome Telescope is a 40cm telescope located at DoA Dome Observatory in Peking University, Beijing, China. The detector is a 36mm×24mm QHY-11 CCD with 9um pixels, giving a field of view of approaximately 30×20 square arcmins. The data consist of Optical imaging in three broadband filters (B, V, sdss-r) over all pointings. For different star cluster observations, we have multiple exposures at different time epoch for each sources. The observation log is shown in Appendix 1.

3. IMAGE REDUCTION

3.1. *Stage1 – Detector-level Corrections*

Stage 1 of my Calibration Pipeline performs detector-level corrections, many of which are common to all instruments and observing modes. This stage of reduction take care of instrumental contaminations on the CCD chip, including bias, dark, and flat field corrections.

3.1.1. *Bias Subtraction*

For every single image taken by the CCD, there is a bias level that is added to the image. This bias level is a result of the CCD electronics and is independent of the exposure time (might be influenced by the temperature of the electronics). The bias level is measured by taking a zero-length exposure, which is an exposure with zero exposure time. The bias level is then subtracted from every image taken by the CCD. This step is actually done by Professor Wang Ran, and I just use the bias subtracted images in the following steps.

3.1.2. *Dark Subtraction*

Dark subtraction is a process that removes the dark current from the CCD. The dark current is a result of thermal electrons in the CCD that are generated by the heat of the CCD. The dark current is measured by taking a series of exposures with the same exposure time as the science images, but with the shutter closed. This step is again done by Professor Wang Ran, and I just use the dark frame for each exposure time to subtract the dark current from the science images.

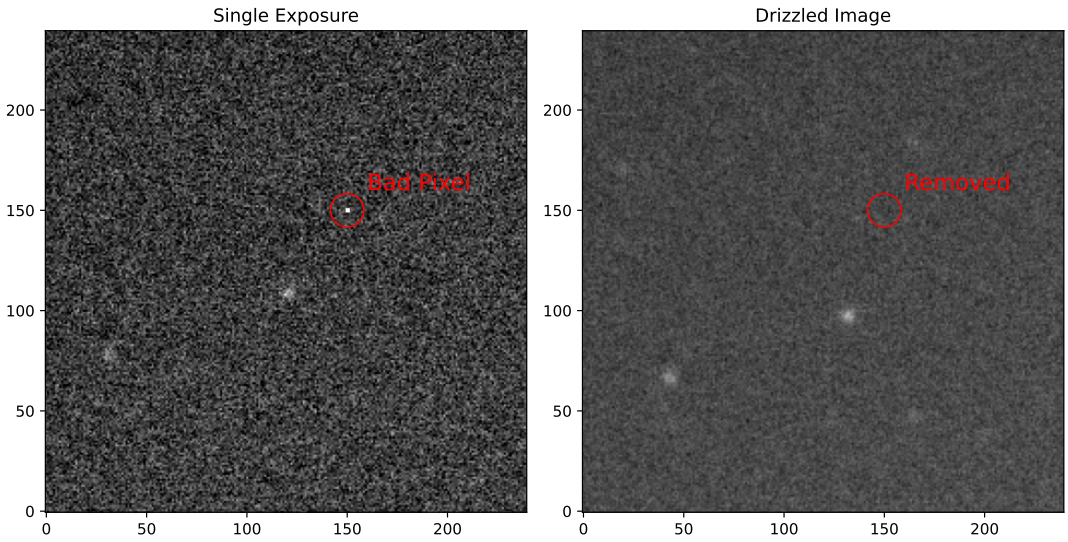

Figure 1. The result of drizzle. The left panel shows the raw image before drizzle, and the right panel shows the image after drizzle. The image quality is improved after drizzle, including the removal of bad pixels and the improvement of the signal-to-noise ratio.

3.1.3. *Flat Correction*

Flat correction is a process that corrects for pixel-to-pixel sensitivity variations across the CCD. The flat correction is performed by dividing each image by a normalized flat field image. Again here, the flat field image is provided by Professor Wang Ran, with dark and bias subtracted. The flat field image is normalized by dividing the median value of the image. The science images are then divided by the normalized flat field image, directly after the dark subtraction step.

3.2. *Stage2 – Individual Image Calibrations*

Stage 2 of my Calibration Pipeline performs calibrations that are specific to individual images. These calibrations are performed on each image independently of all other images.

3.2.1. *Source Detection*

Source detection is a pre-process for astrometric calibration and flux calibration. The source detection is performed by using the DAOStarFinder, which is a Python package in Photutils[1]. The DAOStarFinder is a source detection algorithm that uses a 2D Gaussian function to fit the sources in the image (Stetson 1987). Considering the fact that stars in the image are not perfect point sources due to PSF and most importantly, the seeing effect, I set the FWHM of the DAOStarFinder input to be 10 pixels, which is approximately the FWHM of the stars in the image revealed by software SAOImageDS9. However, since the seeing is not constant during the observation among different nights, the choice of FWHM, should be under careful consideration. 10 pixels is proved to be a good choice by the result of source detection shown in Figure 3.

The detection threshold is set to be 15σ above the background estimated by the mode estimator for sdss-r and V band, and 12σ for B band. The background variance is estimated by the standard deviation after sigma-clipping.

3.2.2. *Astrometric Calibration*

Astrometric calibration is a process that converts the pixel coordinates of sources in the image to the sky coordinates (RA, Dec). The astrometric calibration is performed by using the astrometry.net[2] package (Lang et al. 2010). With the source catalog at hand, the astrometry.net package will match the sources with given initial parameters and return the wcs solution. To test the accuracy of the astrometric calibration, I crossmatch the sources with the reference catalog from the APASS (Henden et al. 2018). More details will be described in Section 3.3.2.

3.3. *Stage3 – Ensemble Processing*

Stage 3 of my Calibration Pipeline performs science-level calibrations to ensemble images. These calibrations are performed on all available images together, and are therefore able to take advantage of the statistical properties of the ensemble.

[1] https://photutils.readthedocs.io/en/stable/

[2] https://astrometry.net/

Figure 2. The pseudo-color image of M52. Blue represents B band, yellow is filled with V band, and red is sdss-r band.

3.3.1. *Drizzle*

After assigning WCS information to individual images, I am able to combining 'dithered' images into a single image. The reason I use the phrase 'dithered' is because the images are not dithered intentionally, but the telescope is not tracking the target perfectly, so the images are dithered unintentionally, which, however, is good for combining images. Drizzle is a linear reconstruction of an image from undersampled, dithered data. It can weight input images according to the statistical significance of each pixel, and removes the effects of geometric distortion both on image shape and photometry (Fruchter & Hook 2002). The combining process is performed by using the Drizzle package powered by Astropy. The drizzle package is able to combine images with different pixel scales and orientations. This step is necessary because the image quality is heavily defected by CCD defects and seeing effect. The final image is shown in Figure 1. The image shows that the image quality is improved after drizzling, including the removal of bad pixels and the improvement of the signal-to-noise ratio.

With the drizzled image in hand, I combine these 3 band images to a pseudo-color image, which is shown in Figure 2.

3.3.2. *Crossmatch*

To calibrate physical properties of the sources in the image, I need to crossmatch the sources with the reference catalog from APASS. I do not use source detected from the individual images from the previous step 3.2.1 because the image quality is not satisfying. Instead, I use the source detected from the drizzled image. The detection result is shown in Figure 3.

The AAVSO Photometric All-Sky Survey (APASS) performed an allsky photometric survey in 5 filters: Johnson B and V, sdss-g, sdss-r and sdss-i. Since APASS has the same filters as our observation, it should be a good reference catalog for our observation.

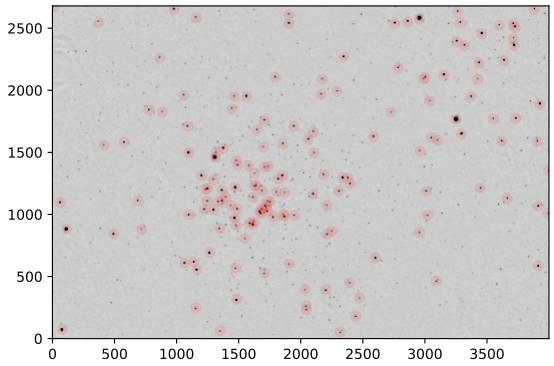

Figure 3. The result of source detection. The choice the detection FWHM is proved to be satisfying.

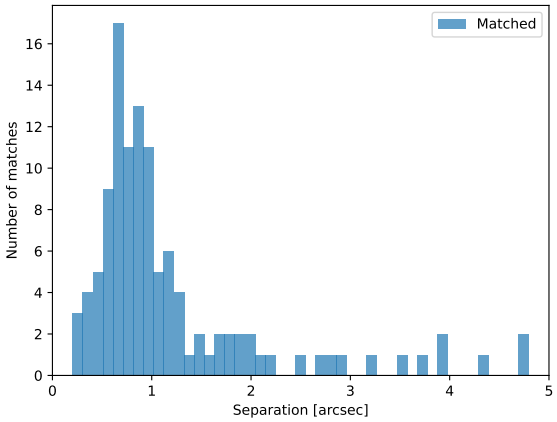

Figure 4. The distribution of separation between sources and the reference catalog. There are totally 134 number of matches (including the target variable). Most matches are within 1.6 arcsec.

The crossmatch is performed by using the Astropy[3] package. The final crossmatch result is shown in Figure 4.

The distribution shows that the separation to the reference catalog is less than 1.6 arcsec for most sources, indicating a satisfying astrometric calibration.

3.3.3. *Flux Calibration*

[3] http://www.astropy.org

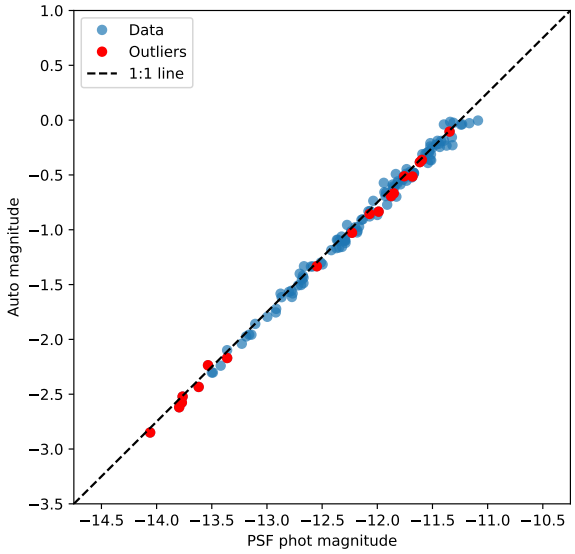

Figure 5. The comparison between auto magnitude given by the DAOStarFinder and PSF magnitude in sdss-r band. The red dots represent the excluded sources from the flux calibration.

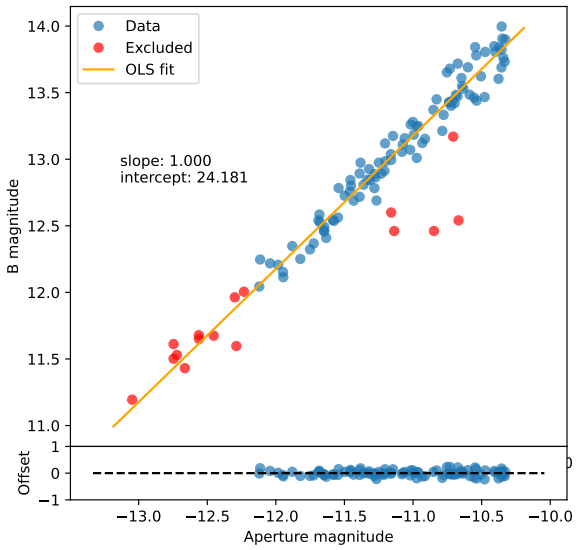

Figure 6. The result of Flux calibration in B band. The red dots represent the excluded sources from the flux calibration.

Flux calibration is a process that converts the instrumental magnitude of sources in the image to the calibrated magnitude.

When capturing star clusters, which is relatively birght and crowded, the aperture photometry is not a good choice because the flux from neighboring sources will contaminate the flux from the target source. Meanwhile, the birghtest sources in the images are saturated, which means the flux from these sources are not reliable. So I choose to use the PSF photometry method to measure the flux of the sources.

To perform PSF photometry, I first need to construct the PSF model. The PSF model is constructed by using the Integrated Gaussian PRF with a sigma of 6.0 pixel. The fitting shape is the central 17×17 pixels of the DAOStarFinder output source positions. I use an annulus local background estimator to estimate the background level. The inner radius of the annulus is 17.5 pixels, and the outer radius is 20 pixels. The initial guess of the PSF model flux is the flux of the source in the 16 pixel radius aperture.

The choice of configuration above is proved to be satisfying by the comparison between auto magnitude given by the DAOStarFinder, according to Figure 5.

With a robust photometry, I calibrate the zeropoint by regressing the instrumental magnitude with the reference catalog. The calibration is based on catalog provided by APASS. I exclude the sources which are saturated or with bad PSF fitting results. The result of Flux calibration is shown in Figure 6.

I finally derive the zeropoint in B,V and sdss-r band respectively:

$$\text{ZEROPOINT} = 24.181 \pm 0.244 \quad \text{in} \quad \text{B} \quad \text{band} \tag{1}$$

$$\text{ZEROPOINT} = 23.788 \pm 0.198 \quad \text{in} \quad \text{V} \quad \text{band} \tag{2}$$

$$\text{ZEROPOINT} = 24.547 \pm 0.187 \quad \text{in} \quad \text{sdss} - \text{r} \quad \text{band} \tag{3}$$

4. KNOWN ISSUES

4.1. *Error Budget*

The error of photometry cannot be calculated directly from the science data. I need to construct an error map for science image with not only science frame itself, but flat frame, dark frame and bias frame as well. However, since I cannot obtain the readnoise from the detector, it's hard to only construct the error map with the poisson noise. And the error will propogate during the calibration process including drizzling.

Another problem is when doing PSF photometry, the error cannot be calculated from a naive way. I may need to do mock analysis to estimate the error, which is far beyond the course. In this case, I cannot give a reliable error budget for the photometry. This should be improved in the future.

4.2. *Sources thrown away*

There are some sources thrown away during the calibration process. This will lead to a smaller number of sample in the final result. The reason for throwing away is that the sources are in the marginal region of the image, can be cut during the drizzling process, or cannot be used because of the defect of the CCD. The former can be improved by changing the drizzle parameters in the future.

5. RESULTS

5.1. *Sky background and Imaging Sensitivity*

The Sky background can be estimated with the zero point of the flux measurement. At a single background pixel, the magnitude of the sky in mag/arcsec^2 can be calculated by the following equation 4.

$$m_{sky} = -2.5log(ADU) + \text{ZEROPOINT} \tag{4}$$

where ADU is the ADU value of the background pixel. I use the median value of the global background as the typical value. However, because there is a gradual change of the background in the field, the sky brightness may not be uniform. The sky background is estimated to be $m_{sky} = 14.411 \pm 0.244\,\text{mag/arcsec}^2$ in B band, $m_{sky} = 13.349 \pm 0.198\,\text{mag/pix}^2$ in V band, and $m_{sky} = 14.219 \pm 0.187\,\text{mag/pix}^2$ in sdss-r band.

The imaging sensitivity is the limiting magnitude of the image, which is the magnitude of the faintest source that can be detected under a given signal-to-noise ratio. Sensitivity estimates can vary significantly depending on the background and the assumed photometric aperture sizes.

The signal-to-noise ratio (SNR) for a point source depends on both the Poisson noise of the object, and on noises associated with the background. Sources of background noise include "read noise" of the CCDs, and Poisson noise in the dark current, sky background. Here for simplicity, I only consider the Poisson noise from the sky background and the object.

Under a given signal-to-noise ratio $SNR = 5$ at 30 seconds exposure time, with an aperture size of 15 pixels and a specific sky background at given epoch, the limiting magnitude can be calculated as follows. The aperture size is quite crucial in determining the limiting magnitude though. Considering that our seeing disc has FWHM larger than 3 arcsec, I choose the aperture size to be 15 pixels, which is approximately a robust aperture to include all the signals. The signal-to-noise ratio is calculated by the following equation:

$$SNR = \frac{N_S}{\sqrt{N_S + n_{pix}\left[(N_{bk} + N_{dk})/5 + readnoise^2\right]}} \tag{5}$$

where N_S represents ADUs collocted from sources, N_{bk} is from the sky background and N_{dk} is from the dark current. n_{pix} is the total pixel number used to calculate aperture photometry. The reason I divide n_{pix} by 5 is that when coadding 5 images, the noise will be reduced by a factor of $\sqrt{5}$. But the readnoise will not be reduced, which is estimated by typical QHY11 CCD readnoise value of 12-16 ADU. By assuming the threshold $SNR = 5$, I can derive the limiting magnitude for each band

$$m_{lim} = -2.5log(ADU) + \text{ZEROPOINT} \tag{6}$$

where ADU satisfy:

$$ADU = \frac{SNR}{2}\left[SNR + \sqrt{SNR^2 + 4n_{pix}(...)}\right] \tag{7}$$

The limiting magnitude is estimated to be $m_{lim} = 15.334 \pm 0.244$ mag in B band, $m_{lim} = 14.781 \pm 0.198$ mag in V band, and $m_{lim} = 15.520 \pm 0.187$ mag in sdss-r band. This is quite consistent with my sample selection, where I have my sample brighter than 14.5 mag in all bands, as shown in Figure 8, satisfying signal-to-noise ratio larger than 5.

5.2. *Confirm Stellar Members of M52*

Before finally deriving the Hertzsprung-Russell Diagram, I need to confirm whether the sources in the image are stellar members of M52. I adopt an open cluster member catalog from Cantat-Gaudin et al. (2018). The catalog contains 112 stellar members of M52. I cross-match the sources in the image with the catalog and find 86 matches. The result is shown in Figure 7.

5.3. *Reddening Correction and Absolute Magnitude*

Before considering intrinsic properties of star cluster, I can only derive the apparent magnitude and color of the sources, as shown in Figure 8.

I adopt the distance modulus of $\mu = 13.20 \pm 0.16$ mag, and color excess $E(B-V) = 0.57 \pm 0.04$ mag from Akbulut et al. (2021). The extinction coefficient I use is the well-known Milky Way extinction $R_V = 3.1$ (Schultz & Wiemer 1975). After correcting for reddening and extinction, I derive the absolute magnitude and intrinsic color of M52, shown in Figure 9.

6. DISCUSSION

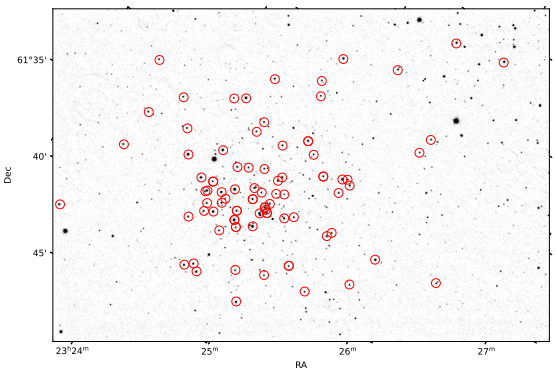

Figure 7. The members of open cluster M52 crossmatched with the reference catalog (Cantat-Gaudin et al. 2018). There are totally 86 number of matches. Most matches are within 1.6 arcsec.

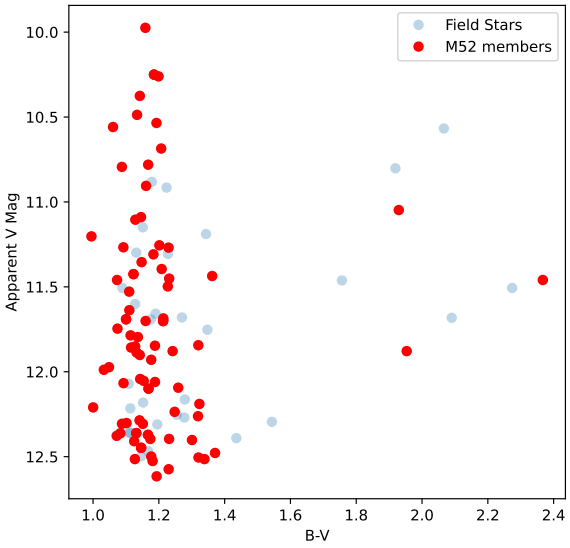

Figure 8. The apparent magnitude and color of field stars. The brightest source may not be credible because of saturation.

6.1. *Hertzsprung-Russell Diagram of M52*

Combining with the result from Pandey et al. (2001), I plot the complete Hertzsprung-Russell Diagram of M52 in Figure 10. The result shows that the color and magnitude measured by DoA Dome Telescope is consistent with the previous measurement.

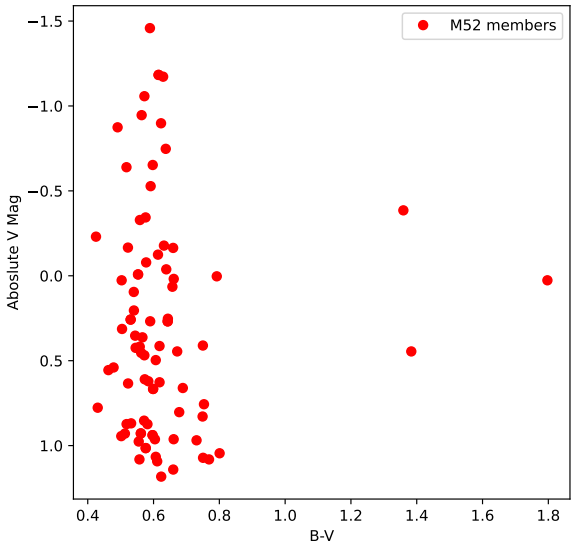

Figure 9. The absolute magnitude and intrinsic color of M52 members. The brightest source may not be credible because of saturation.

From Figure 10, our DoA Dome Telescope can only reveal the tip of an iceberg. The image is not deep enough to reveal the whole main sequence of M52. However, I can still conclude that my measurement has agreed well with the previous measurement, at least for brightest sources in the cluster.

There is no prominent turn-off point nor giant branch in the Hertzsprung-Russell Diagram, which means that M52 is quite a young cluster, whose brightest stars are mostly still on the main sequence. Considering the timescale for the brightest stars to evolve off the main sequence is about 20 million years, and I do find some stars off the main sequence, the age of M52 is estimated to be a little larger than 20 million years.

Thank Professor Wang Ran for providing the data and some of the first stage reduction product.

Facilities: DoA Dome Telescope

Software: astropy (Astropy Collaboration et al. 2013), photutils (Bradley et al. 2023), astrometry.net Lang et al. (2010)

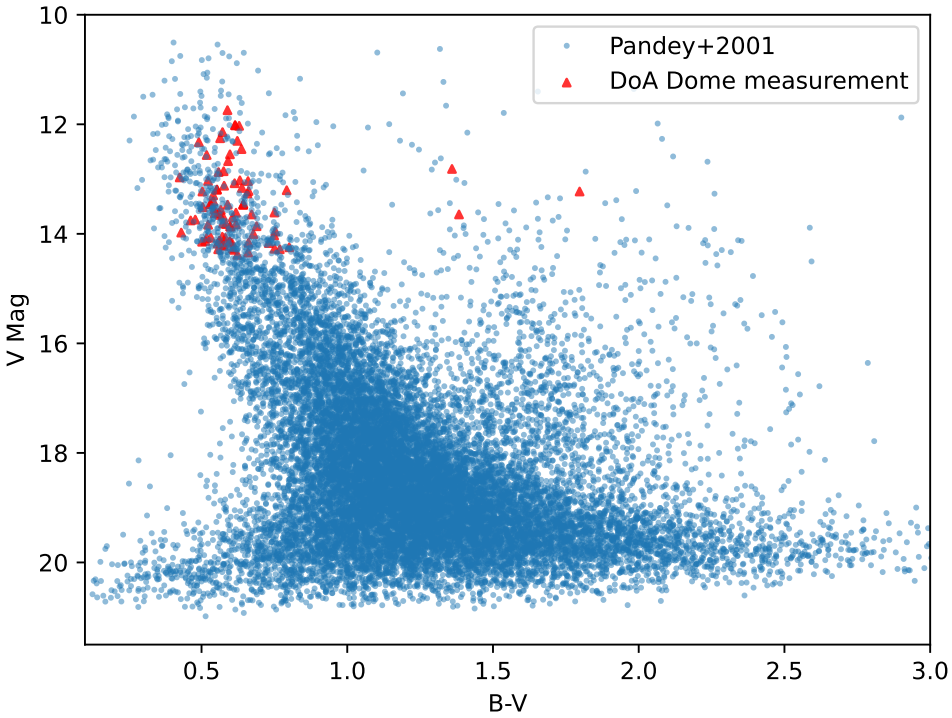

Figure 10. The Hertzsprung-Russell Diagram of M52. The result shows that the light curve measured by DoA Dome Telescope is consistent with the previous measurement, though the data can only show the tip of an iceberg. Pandey et al. (2001) didn't include distance modulus, so I subtract it back from the absolute magnitude.

APPENDIX

A. OBSERVATION LOG

The observation log is shown in Table 1. The exposures at different time epoch are drizzled together to form a single image. The images I use in this work are all from the later epoch, which is because the later epoch has better image quality.

Table 1. Observation Log

Object	Filter	Exposure Time (s)	Number of Exposures	Date	Time
M 52	B	30	5	2023-09-25	19:49:19
M 52	V	30	5	2023-09-25	19:53:05
M 52	sdss-r	30	5	2023-09-25	19:56:50
M 52	B	30	5	2023-09-25	20:13:59
M 52	V	30	5	2023-09-25	20:18:28
M 52	sdss-r	30	5	2023-09-25	20:22:14

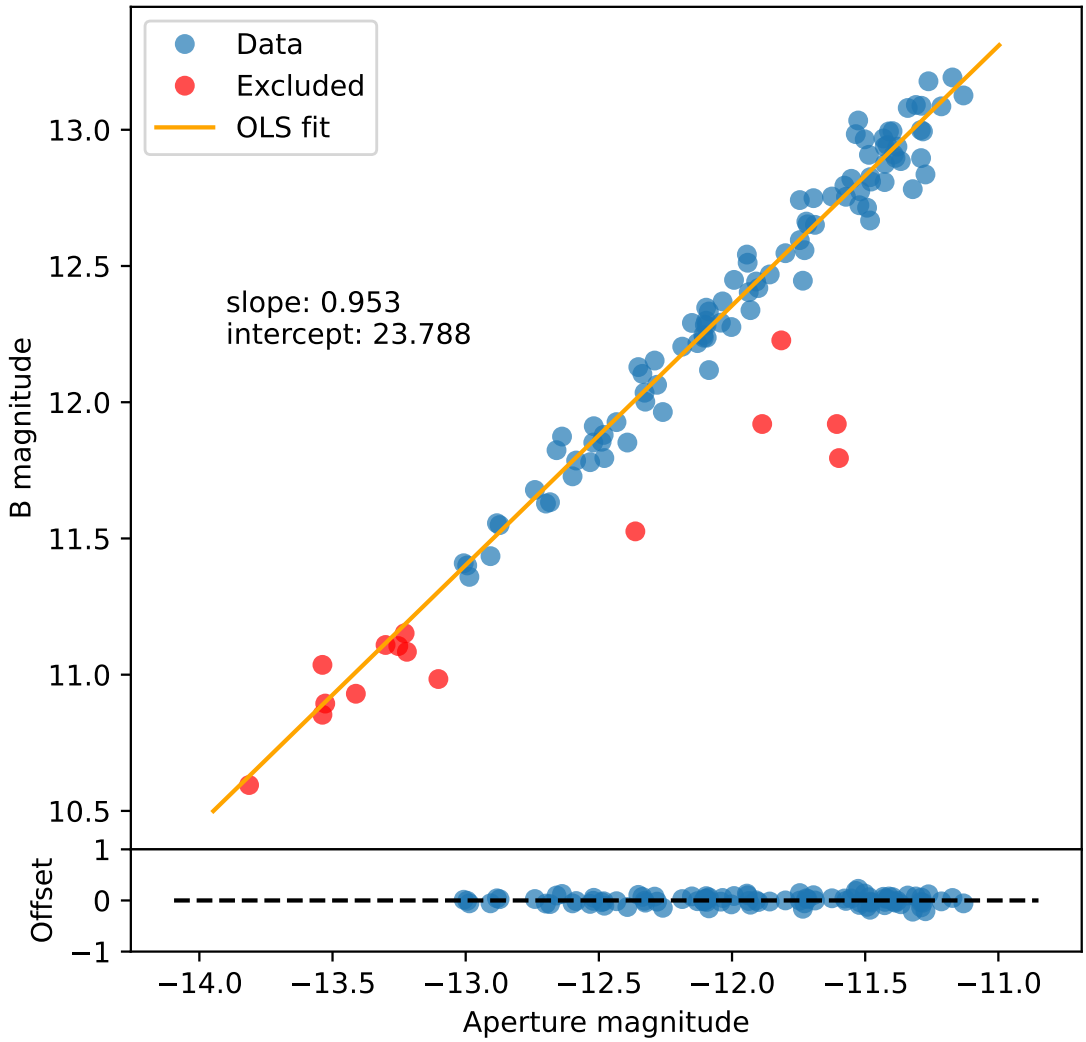

Figure 11. The result of Flux calibration in V band. The red dots represent the excluded sources from the flux calibration.

B. FLUX CALIBRATION ON OTHER BANDS

Zeropoint calibration is performed on other bands as well. The result is shown in Figure 11 and Figure 12.

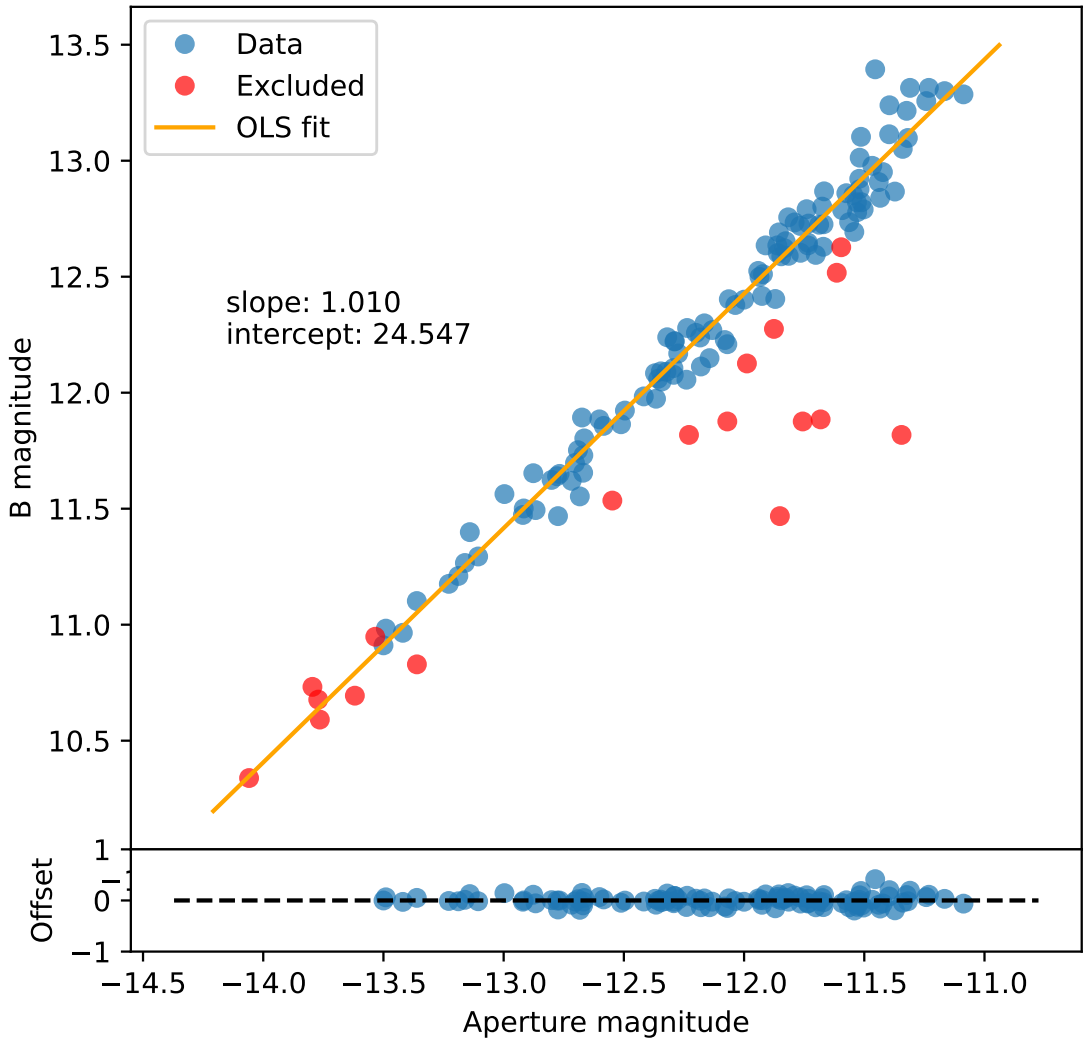

Figure 12. The result of Flux calibration in sdss-r band. The red dots represent the excluded sources from the flux calibration.

C. MAGNITUDE-COLOR DIAGRAM OF M52

I have also calibrated data in sdss-r band. Figure 13 shows the result.

REFERENCES

Akbulut, B., Ak, S., Yontan, T., et al. 2021, Ap&SS, 366, 68, doi: 10.1007/s10509-021-03975-x

Astropy Collaboration, Robitaille, T. P., Tollerud, E. J., et al. 2013, A&A, 558, A33, doi: 10.1051/0004-6361/201322068

Bradley, L., Sipőcz, B., Robitaille, T., et al. 2023, astropy/photutils: 1.10.0, 1.10.0, Zenodo, doi: 10.5281/zenodo.1035865

Cantat-Gaudin, T., Jordi, C., Vallenari, A., et al. 2018, A&A, 618, A93, doi: 10.1051/0004-6361/201833476

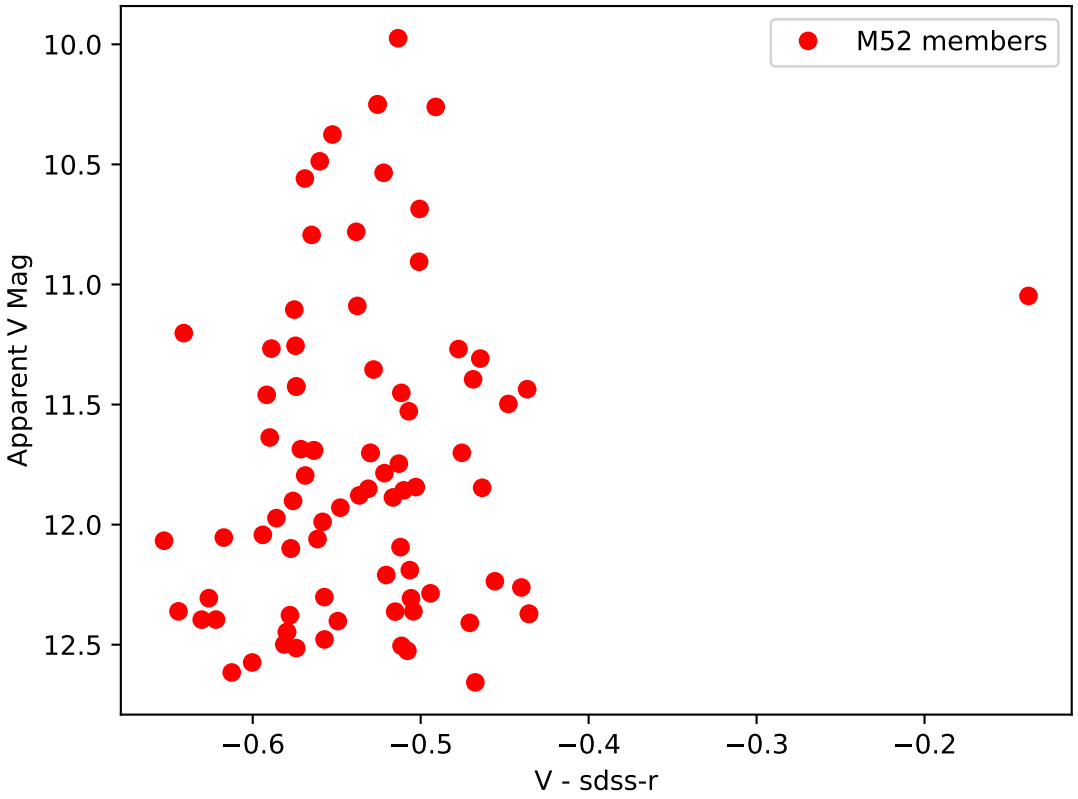

Figure 13. The Color-Magnitude Diagram of M52. The result shows the V - sdss-r color and apparent V magnitude measured by DoA Dome Telescope.

Fruchter, A., & Hook, R. 2002, Publications of the Astronomical Society of the Pacific, 114, 144–152, doi: 10.1086/338393

Henden, A. A., Levine, S., Terrell, D., et al. 2018, AAVSO Photometric All Sky Survey (APASS) DR10, VO resource provided by the GAVO Data Center. http://dc.zah.uni-heidelberg.de/apass/q/cone/info

Lang, D., Hogg, D. W., Mierle, K., Blanton, M., & Roweis, S. 2010, The Astronomical Journal, 139, 1782–1800, doi: 10.1088/0004-6256/139/5/1782

Pandey, A. K., Nilakshi, O. K., Sagar, R., & Tarusawa, K. 2001, VizieR Online Data Catalog, J/A+A/374/504, doi: 10.26093/cds/vizier.33740504

Schultz, G. V., & Wiemer, W. 1975, A&A, 43, 133

Stetson, P. B. 1987, PASP, 99, 191, doi: 10.1086/131977